AIAA JOURNAL
Vol. 38, No. 6, June 2000

Dynamic Stability of a Free–Free Cylindrical Shell Under a Follower Force

Si-Hyoung Park* and Ji-Hwan Kim†
Seoul National University, Seoul 151-742, Republic of Korea

The dynamic stability of a completely free isotropic circular cylindrical shell under a follower force is investigated. The first-order shear deformation and rotary inertia are included in the kinetic energy and the strain energy. A finite element model of the shell is formulated using the trigonometric ring element in the circumferential direction and the Lagrangian element in the longitudinal direction. Using the eigenvalue curves and the method of multiple scales, the dynamic stability is studied for the case of the follower force with a pulsating part as well as the constant follower force. The effect of the thickness ratio and the length ratio is presented in both cases. The numerical results for the shells are compared with those of a beam model having equivalent dimensions. The numerical results show that the shell under a constant follower force behaves like a beam in a certain range. The analysis of the shell under a pulsating follower force shows that the beamlike modes of the shell have larger unstable regions than the other modes. However, for the case of a pulsating load, the modes of higher circumferential wave number are of importance in that the combination resonance of difference type takes place frequently.

Nomenclature

E	= Young's modulus
L, h, R	= length, thickness, and radius of a shell
$\boldsymbol{M}^{(m)}$, $\boldsymbol{K}^{(m)}$, $\boldsymbol{S}^{(m)}$	= dimensional mass, stiffness, and geometric stiffness matrices
$\bar{\boldsymbol{M}}^{(m)}$, $\bar{\boldsymbol{K}}^{(m)}$, $\bar{\boldsymbol{S}}^{(m)}$	= nondimensionalized mass, stiffness, and geometric stiffness matrices
P_0	= magnitude of constant part of a follower force
P_1	= magnitude of pulsating part of a follower force
$\boldsymbol{Q}$	= material stiffness matrix for plane stress
T	= kinetic energy
u_0, v_0, w_0	= displacements of the middle surface in the x, ϑ, and z directions
V	= strain energy
$\bar{\boldsymbol{X}}^{(m)}$	= generalized coordinate (nondimensionalized)
$\boldsymbol{X}^{(m)}$	= generalized coordinate (dimensional)
$y_p^{(m)}$	= orthogonalized coordinate
$\beta_{\rm cr}$	= nondimensionalized critical load
$\beta(t)$	= nondimensionalized follower force [see Eq. (13)]
β_0	= nondimensionalized constant part of a follower force [see Eq. (17)]
β_1	= nondimensionalized pulsating part of a follower force [see Eq. (21)]
ε	= strain tensor [see Eq. (4)]
ϵ_0	= constant load parameter [see Eq. (20a)]
ϵ_1	= pulsating load parameter [see Eq. (20b)]
Λ_{pq}	= bandwidth parameter
λ	= nondimensionalized natural frequency
λ_f	= nondimensionalized driving frequency [see Eq. (19)]
ν	= Poisson's ratio for shell material
ρ	= material density (mass/volume)
σ	= stress tensor [see Eq. (5)]
τ	= nondimensionalized time [see Eq. (14)]
φ, ψ	= change of slope of the normal to the middle surface
ω_f	= driving frequency

Received 19 April 1999; revision received 21 September 1999; accepted for publication 21 September 1999.

*Research Assistant, Department of Aerospace Engineering, College of Engineering, Shinrim-Dong, Gwanak-Gu.
†Associate Professor, Department of Aerospace Engineering, College of Engineering, Shinrim-Dong, Gwanak-Gu. Member AIAA.

Introduction

A FREE–FREE beam or a completely free plate model has been used to study the dynamic stability of flexible aerospace structures and missiles. On the other hand, though the cylindrical shell is one of the basic elements commonly used in aerospace structures, the investigation of completely free shells under a follower force has not been carried out.

Much attention has been focused on free–free beams subjected to a follower force. Beal[1] first investigated a free–free beam under a constant thrust and a pulsating thrust using the Euler–Bernoulli beam theory. In his work, the instability types under a constant follower force were divided into two categories, namely, a flutter type and a divergence type. Wu,[2] Park and Mote,[3] and Park[4] examined the dynamic instability of a free–free beam in the various aspects for the case of a constant follower force. Wu[2] studied the relation between the critical load and the eigencurves using the finite element method. Park and Mote[3] investigated the effect of a concentrated mass on the critical load and the instability type. Park[4] treated a beam model with various rotary inertia and shear deformation parameters using the finite element method. Kim and Choo[5] discussed the dynamic instability of a free–free beam subjected to a pulsating follower force using the Timoshenko beam theory. They used the method of multiple scales and studied the effect of the various parameters on the parametric instability region. The effect of a concentrated mass was also treated.

Several papers on the dynamic stability of plates under a follower force are also available. However, works about the plate model treated only the constant loads. A completely free plate subjected to a follower force was studied by Higuchi and Dowell.[6,7] They classified the plates into two categories, namely, beamlike plates and rectangular plates. In these papers, the effect of damping on stability was also investigated. Kim and Park[8] treated the problem for various locations and magnitudes of intermediate follower forces using the finite element method.

Works on the stability of cylindrical shells have been performed only for the case of conservative loads. In addition, most of these works did not include the completely free edge condition. Lam and Ng[9] investigated the dynamic stability of a cylindrical shell under a pulsating axial load. They examined the simply supported shells using the various thin-shell theories for the governing equations and Bolotin's method for the study of the parametric resonances. Bismarck[10] dealt with the dynamic stability of a shell under a follower force. In addition to the free edge condition, various boundary conditions were treated in this paper. However, this paper deals with a shallow shell rather than a completely cylindrical shell and treats only a constant load.

In the present work, the dynamic stability of completely free isotropic cylindrical shells under follower forces is studied using the finite element method. The shear deformation energy and the rotary inertia are included in the potential energy and the kinetic energy. The unperturbed stress distribution is assumed to be uniform through the thickness and to be linear along the longitudinal direction. Because the rigid-body mode cannot be reproduced by using the Lagrangian element in the shell coordinate, the trigonometric ring element in the circumferential direction and the four-node Lagrangian element in the longitudinal direction are used. The dynamic stability is studied for the case of a constant follower force and a pulsating force, respectively. For the case of a constant load, the eigenvalue curves are used to obtain the critical load. A completely free shell has Rayleigh modes and Love modes as the two lowest modes when the number of circumferential waves is equal to or greater than two.[11] Because the critical load is related to the lowest eigenvalues, the Rayleigh mode and the Love mode may have an effect on the stability of shells. For the case of the follower force with a pulsating part, the method of multiple scales is used to obtain the transition curves separating stable from unstable regions. The results for both the constant load and the pulsating load are calculated for various length and thickness ratios. A beam model corresponding to the shell is analyzed and compared with the results of the shell model.

Basic Equations

Figures 1a and 1b show a circular cylindrical shell of length L, thickness h, and radius R. The XYZ axis and the $x\vartheta z$ axis are the inertial coordinate and the curvilinear coordinate of a shell, respectively. The x axis is taken along a generator, the circumferential arc length subtends an angle ϑ, and the z axis is directed radially outwards. A follower force with the magnitude $P(t)$ is assumed to be uniformly distributed along an edge at $x = 0$ and to be collinear with the deformed generator.

Basic equations are derived by making the following assumptions:

1) The deflections are small.

2) The material is elastic and isotropic.

3) The transverse shear strains are constant through the thickness.

4) The direction of a follower force is not controlled.

For the shell dimensions ($h/R < 0.2$) considered in the present analysis, the thin-shell theories cannot produce good results, and the high-order theory is not much better than the first-order theory in accuracy as shown in Ref. 12. Therefore, considering the computational efficiency, we include only first-order shear deformation and rotary inertia. The displacement field can be written as[13]

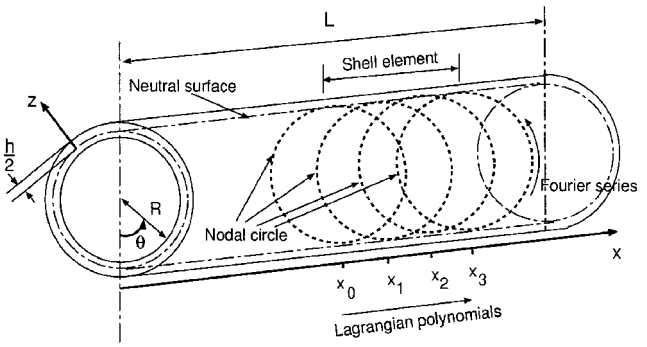

Fig. 1a Coordinate system and cylindrical shell element.

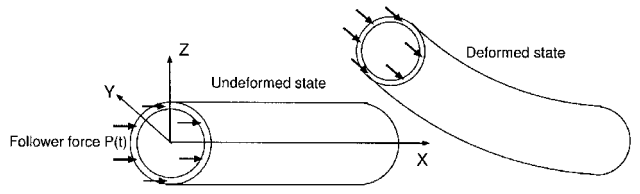

Fig. 1b Configuration of shell and follower force.

$$u = u_0(x, \vartheta, t) + z\varphi(x, \vartheta, t) \tag{1a}$$

$$v = v_0(x, \vartheta, t) + z\psi(x, \vartheta, t) \tag{1b}$$

$$w = w_0(x, \vartheta, t) \tag{1c}$$

Using the preceding displacement fields, we get the kinetic energy as

$$T = \frac{1}{2}\rho \int_0^{2\pi}\int_0^{L}\int_{-h/2}^{h/2} \left(\dot{u}_0^2 + \dot{v}_0^2 + \dot{w}_0^2 + 2z\dot{u}_0\dot{\varphi} + 2z\dot{v}_0\dot{\psi} + z^2\dot{\varphi}^2 + z^2\dot{\psi}^2\right)(R + z)\,\mathrm{d}z\,\mathrm{d}x\,\mathrm{d}\vartheta \tag{2}$$

The strain energy is expressed as

$$V = \frac{1}{2}\rho \int_0^{2\pi}\int_0^{L}\int_{-h/2}^{h/2} \varepsilon^T \boldsymbol{Q}\varepsilon(R + z)\,\mathrm{d}z\,\mathrm{d}x\,\mathrm{d}\vartheta \tag{3}$$

The strain ε, the stiffness $\boldsymbol{Q}$, and the displacement fields have the following relation to each other:

$$\varepsilon = \begin{bmatrix} \epsilon_{xx} \\ \epsilon_{\vartheta\vartheta} \\ \gamma_{x\vartheta} \\ \gamma_{xz} \\ \gamma_{\vartheta z} \end{bmatrix} = \begin{bmatrix} \dfrac{\partial u_0}{\partial x} + z\dfrac{\partial \varphi}{\partial x} \\ \dfrac{1}{R+z}\left(\dfrac{\partial v_0}{\partial \vartheta} + w_0\right) + \dfrac{z}{R+z}\dfrac{\partial \psi}{\partial \vartheta} \\ \dfrac{\partial v_0}{\partial x} + z\dfrac{\partial \psi}{\partial x} + \dfrac{1}{R+z}\dfrac{\partial u_0}{\partial \vartheta} + \dfrac{z}{R+z}\dfrac{\partial \psi}{\partial \vartheta} \\ \varphi + \dfrac{\partial w_0}{\partial x} \\ \psi + \dfrac{1}{R+z}\left(\dfrac{\partial w_0}{\partial \vartheta} - v_0\right) - \dfrac{z}{R+z}\psi \end{bmatrix} \tag{4}$$

$$\sigma = \begin{bmatrix} \sigma_{xx} \\ \sigma_{\vartheta\vartheta} \\ \sigma_{x\vartheta} \\ \sigma_{xz} \\ \sigma_{\vartheta z} \end{bmatrix} = \boldsymbol{Q}\varepsilon$$

$$= \begin{bmatrix} \dfrac{E}{(1-\nu^2)} & \dfrac{\nu E}{(1-\nu^2)} & 0 & 0 & 0 \\ & \dfrac{E}{(1-\nu^2)} & 0 & 0 & 0 \\ & & \dfrac{E}{2(1+\nu)} & 0 & 0 \\ & SYM & & \dfrac{kE}{2(1+\nu)} & 0 \\ & & & & \dfrac{kE}{2(1+\nu)} \end{bmatrix}$$

$$\times \begin{bmatrix} \epsilon_{xx} \\ \epsilon_{\vartheta\vartheta} \\ \gamma_{x\vartheta} \\ \gamma_{xz} \\ \gamma_{\vartheta z} \end{bmatrix} \tag{5}$$

The stiffness matrix $\boldsymbol{Q}$ includes the shear correction factor k and the material properties. Equation (4) shows the linear strain-displacement relation and is based on the work of Soedel.[13]

The extended Hamilton's principle is applied to a shell subjected to a tangential follower force as follows:

$$\int_{t_1}^{t_2} (\delta T - \delta V + \delta W_f)\,\mathrm{d}t = 0 \tag{6}$$

If we assume that the effect of axial vibration is negligible and that the unperturbed stress σ_{xx} is uniformly distributed in the thickness direction, δW_f is expressed as

$$\delta W_f = \int_0^{2\pi}\int_0^L \frac{P(t)}{L}(L-x)\left(\frac{\partial \delta w_0}{\partial x}\frac{\partial w_0}{\partial x} + \frac{\partial \delta v_0}{\partial x}\frac{\partial v_0}{\partial x}\right)R\,\mathrm{d}x\,\mathrm{d}\vartheta + \int_0^{2\pi} P(t)\left(\delta w_0\frac{\partial w_0}{\partial x} + \delta v_0\frac{\partial v_0}{\partial x}\right)R\,\mathrm{d}\vartheta|_{x=0} \quad (7)$$

where the rigid-body acceleration of the shell is taken into account by the linear distribution of unperturbed axial stress.[14]

In the present analysis, the dynamic stability is examined for two special cases of $P(t)$. First, $P(t)$ has a constant magnitude as

$$P(t) = P_0 \quad (8)$$

Second, $P(t)$ has a harmonically pulsating part as well as a constant part as

$$P(t) = P_0 + P_1\cos(\omega_f t) \quad (9)$$

The dynamic instabilities of the two cases are very different from each other in the aspect of the method of analysis and the physical meaning.

Method of Analysis

To solve Eq. (6) of variational form, we introduce the base functions as[13]

$$u_0 = \sum_{n=1}^{N}\sum_{m=0}^{\infty} L_n(x)\cos(m\vartheta)U_n^{(m)}(t) \quad (10a)$$

$$v_0 = \sum_{n=1}^{N}\sum_{m=0}^{\infty} L_n(x)\sin(m\vartheta)V_n^{(m)}(t) \quad (10b)$$

$$w_0 = \sum_{n=1}^{N}\sum_{m=0}^{\infty} L_n(x)\cos(m\vartheta)W_n^{(m)}(t) \quad (10c)$$

$$\varphi = \sum_{n=1}^{N}\sum_{m=0}^{\infty} L_n(x)\cos(m\vartheta)\Phi_n^{(m)}(t) \quad (10d)$$

$$\psi = \sum_{n=1}^{N}\sum_{m=0}^{\infty} L_n(x)\sin(m\vartheta)\Psi_n^{(m)}(t) \quad (10e)$$

These displacement functions are based on a Fourier series in the circumferential direction as shown in Fig. 1a. In each displacement, either sine or cosine is excluded from the Fourier series due to the orthogonal property about Eq. (6) decoupling sine(cosine) from cosine(sine). In addition, for $m > 0$, a full Fourier series with both sine and cosine produces two modes with the same shape and frequency, and, for $m = 0$, the torsional modes are not critical in stability analysis on account of their large strain energy. Based on these properties, Eqs. (10) are sufficient for the present analysis. However, if a shell is made of composite materials, the sine and cosine in a Fourier series are coupled with each other by the stress–strain relation (5), and, thus, displacement functions should include a full Fourier series.

With the preceding trigonometric base functions in the ϑ direction, we use the four-node piecewise Lagrangian polynomial for $L_n(x)$ as shown in Fig. 1a. The expression is

$$L_n(x) = \frac{\prod_{k\neq i} x - x_k}{\prod_{k\neq i} x_i - x_k}$$

$$n = 3j - 2 + i, \qquad i = 0, 1, 2, 3, \quad \text{for the } j\text{th element} \quad (11)$$

Examining Eq. (7), we can infer that δW_f has the orthogonal property about the circumferential base functions (10) with different m. In other words, the modes with different circumferential wave numbers can be decoupled, and the follower force does not affect the circumferential variation of the motion of the shell. Using this property, the stability analysis can be performed for each circumferential wave number, respectively. If a follower force or the material property of a shell is not distributed axisymmetrically, all of the circumferential wave numbers should be analyzed simultaneously by a coupled form.

Using the finite element method with the preceding base functions, we obtain discrete equations for each circumferential wave number as follows:

$$\boldsymbol{M}^{(m)}\frac{\mathrm{d}^2}{\mathrm{d}t^2}\boldsymbol{X}^{(m)}(t) + \boldsymbol{K}^{(m)}\boldsymbol{X}^{(m)}(t) + P(t)\boldsymbol{S}^{(m)}\boldsymbol{X}^{(m)}(t) = 0 \quad (12)$$

where $\boldsymbol{X}^{(m)}(t)$ is a vector consisting of $U_n^{(m)}(t)$, $V_n^{(m)}(t)$, $W_n^{(m)}(t)$, $\Phi_n^{(m)}(t)$, and $\Psi_n^{(m)}(t)$. The superscript m indicates the circumferential wave number.

By introducing nondimensional parameters such as x/R, z/R, L/R, and h/R, the following parameters are induced:

$$\beta(t) = P(t)(1-\nu^2)/Eh \quad (13)$$

$$\tau = t[E/(1-\nu^2)\rho R^2]^{\frac{1}{2}} \quad (14)$$

Using Eqs. (13) and (14), Eq. (12) can be written as

$$\bar{\boldsymbol{M}}^{(m)}\frac{\mathrm{d}^2}{\mathrm{d}\tau^2}\bar{\boldsymbol{X}}^{(m)}(\tau) + \bar{\boldsymbol{K}}^{(m)}\bar{\boldsymbol{X}}^{(m)}(\tau) + \beta(\tau)\bar{\boldsymbol{S}}^{(m)}\bar{\boldsymbol{X}}^{(m)}(\tau) = 0 \quad (15)$$

Equation (15) can be analyzed by different procedures according to whether or not the follower force has a pulsating part. In the case that the follower force is a constant one that is expressed in Eq. (8), we can obtain the eigenvalue problem from Eq. (15) as follows:

$$\det\left[-\lambda^2\bar{\boldsymbol{M}}^{(m)} + \bar{\boldsymbol{K}}^{(m)} + \beta_0\bar{\boldsymbol{S}}^{(m)}\right] = 0 \quad (16)$$

where

$$\beta_0 = P_0(1-\nu^2)/Eh \quad (17)$$

The stability of the cylindrical shell can be examined by checking the sign and the imaginary part of λ^2. The coalescence of two eigenvalues of Eq. (16) indicates a flutter-type instability, and the eigenvalues become complex numbers. If an eigenvalue of Eq. (16) reduces to zero, a divergence type instability occurs.[1]

In the case of a pulsating follower force such as Eq. (9), Eq. (15) can be regarded as a system of Mathieu–Hill equations, and equations of this type can be analyzed by various methods.[15] Nayfeh and Mook[15] introduced the method of multiple scales, which is numerically simple. Using the method of multiple scales, Eq. (15) should be transformed to the form

$$\frac{\mathrm{d}^2}{\mathrm{d}\tau^2}y_p^{(m)} + \lambda_p^2 y_p^{(m)} + \epsilon_1\cos(\lambda_f\tau)\sum_{q=1}^{M} f_{pq}y_p^{(m)} = 0 \quad (18)$$

where

$$\lambda_f^2 = \omega_f^2[(1-\nu^2)/E]\rho R^2 \quad (19)$$

We take only the constant part of the follower force into account in Eq. (15). In such cases, the eigenvalue problem is obtained as mentioned in the preceding paragraph. Once one obtains the normalized left and right eigenvectors of the eigenvalue problem, the spectral decomposition of the matrices $\bar{\boldsymbol{M}}^{(m)}$ and $\bar{\boldsymbol{K}}^{(m)} + \beta_0\bar{\boldsymbol{S}}^{(m)}$ can be performed. We can obtain Eq. (18) from Eq. (15) by using these procedures and more nondimensional parameters as

$$\epsilon_0 = \beta_0/\beta_{\mathrm{cr}} \quad (20a)$$

$$\epsilon_1 = \beta_1/\beta_{\mathrm{cr}} \quad (20b)$$

where

$$\beta_1 = P_1[(1-\nu^2)/Eh] \quad (21)$$

and β_{cr} is the magnitude of β_0 at which a divergence or a flutter takes place for the case of a constant follower force. Once one obtains the form of Eq. (18), the transition curves in the ϵ_1–λ_f plane separating

stable from unstable regions are defined by the following[15] if λ_f is near $\lambda_p + \lambda_q$ and $f_{pq} f_{qp} > 0$,

$$\lambda_f = \lambda_p + \lambda_q \pm \left(\frac{\epsilon_1}{2}\right)\Lambda_{pq}^{(m)} + \mathcal{O}(\epsilon_1^2), \qquad \Lambda_{pq}^{(m)} = \left(\frac{f_{pq} f_{qp}}{\lambda_p \lambda_q}\right)^{\frac{1}{2}} \tag{22}$$

and if λ_f is near $\lambda_p - \lambda_q$, $f_{pq} f_{qp} < 0$, and $\lambda_p > \lambda_q$,

$$\lambda_f = \lambda_p - \lambda_q \pm \left(\frac{\epsilon_1}{2}\right)\Lambda_{pq}^{(m)} + \mathcal{O}(\epsilon_1^2), \qquad \Lambda_{pq}^{(m)} = \left(\frac{-f_{pq} f_{qp}}{\lambda_p \lambda_q}\right)^{\frac{1}{2}} \tag{23}$$

In the present study, we do not consider a simultaneous occurrence of two resonances and, therefore, the Eqs. (22) and (23) are sufficient for the transition curves. Equations (22) and (23) are the results of first-order expansions for the method of multiple scales. High-order expansions can express the transition curves as more exact and high-order functions. However, if we restrict ϵ_1 within a specific value, first-order expansions also produce a good result as discussed in Ref. 5. In the case $p = q$, the dynamic instability occurring in the region defined by Eq. (22) is called direct parametric resonance. In the other case $p \neq q$, the instability is called combination resonance and is divided into sum type and difference type by the sign of $f_{pq} f_{qp}$ as seen in Eqs. (22) and (23).

Equivalent Beam Model

For the Timoshenko beam theory, nondimensional parameters are the shear deformation parameter $\kappa G A L^2/EI$ and the rotary inertia parameter I/AL^2. In constructing the equivalent beam model, the material properties must be equal to the shell properties, and κ is determined by the shape of the shell cross section as follows[16]:

$$\kappa = \frac{6(1+\nu)(1+\gamma)^2}{(7+6\nu)(1+\gamma)^2 + (20+12\nu)\gamma^2} \tag{24}$$

where

$$\gamma = \frac{1-(h/2R)}{1+(h/2R)} \tag{25}$$

For a circular shell cross section, the rotary inertia parameter can be expressed as

$$I/AL^2 = R^2/2L^2 \tag{26}$$

The shear deformation parameter can be obtained from Eqs. (24) and (26).

Considering that the follower force of the beam is assumed to be a concentrated load and that $P(t)$ in Fig. 1 is a distributed load having the measure of force per unit length, the equivalent nondimensional follower force can be written by means of that of the beam as

$$\beta_{\text{equivalent}}(\tau) = \beta_{\text{beam}}(\tau)[(1-\nu^2)/2](R^2/L^2) \tag{27}$$

Using these parameters, the critical loads of a beam model can be compared with those of a shell model. Comparing the results for the case of a pulsating load, we use the relation between $\Lambda_{pq}^{\text{beam}}$ of a beam and the equivalent value as follows:

$$\Lambda_{pq}^{\text{equivalent}} = \Lambda_{pq}^{\text{beam}} R^2/L^2[(1-\nu^2)/2]^{\frac{1}{2}} \tag{28}$$

Numerical Results

Figure 2 shows the convergence of nondimensional natural frequencies. The analytic solution of these cases is 4×10^{-6} in Ref. 11, in which the solution is based on Flugge's shell theory. In Fig. 2, use of 10 elements can reduce the computational error below 1% in both cases. Considering that the accuracy of the computed frequency is essential to the stability analysis in the present work, 20 elements for the longitudinal direction are enough to get accurate results.

Eight circumferential wave number m from 0 to 7 were considered for the case $P(t) = P_0$, and the critical load was found at the

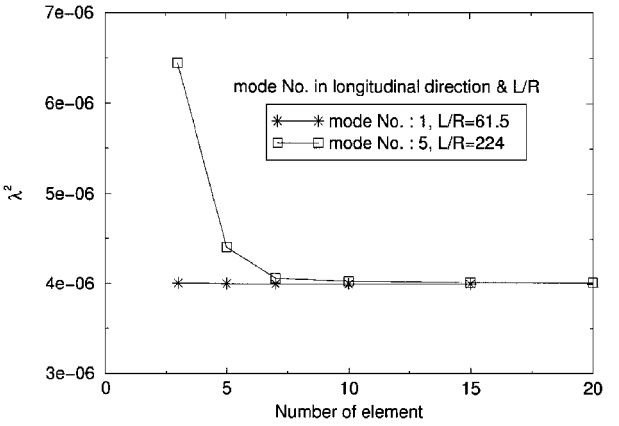

Fig. 2 Convergence of nondimensionalized natural frequencies ($h/R = 0.002$, $m = 2$).

circumferential wave number below $m = 7$ for the shell dimensions considered in this work. In the case $P(t) = P_0 + P_1 \cos(\omega_f t)$, the region of parametric resonance was examined for two circumferential wave numbers ($m = 1$ and 2). This is sufficient to analyze the stability characteristics, because the modes of higher circumferential wave number ($m = 3, 4, \ldots$) have similar mode shapes to the $m = 2$ modes and because the modes ($m = 0, 3, 4, \ldots$) have high frequencies in the range of shell dimensions considered in this paper. For each circumferential wave number, the analysis of parametric instability was performed for the resonances near only the combinations of the first three eigenvalues.

The results for the equivalent beam model were also obtained using the finite element method and compared with those of Refs. 4 and 5. They agreed well with each other; therefore, only the results of the present analysis will be shown in the figures.

Case $P(t) = P_0$ (Constant Load)

The modes of a completely free cylindrical shell can be grouped by the circumferential wave number m. The case $m = 0$ is not examined because the $m = 0$ modes do not induce the critical load. The $m = 1$ modes are beamlike modes and are called first bending mode, second bending mode, and so forth, according to the number of extrema of the mode shape in the longitudinal direction. If $m \geq 2$, the shell has two sets of modes that have a linear or constant axial deformation. The first set, analyzed by Rayleigh, does not vary axially, and the second set, analyzed by Love, has a linear variation.[11] Except for the two sets of modes, the other modes have much bending in the longitudinal direction and are called first bending mode, second bending mode, and so on by the same rule for the case $m = 1$.

Figures 3a and 3b show the typical instability types of completely free shells under a constant follower force. For the shell dimensions considered in the present work, these kinds of flutter instability determine the critical load, although instability of a different type may exist for other dimensions of shells. Because the modes with $m = 1$ are beamlike modes, a beamlike flutter can occur in shells as shown in Fig. 3a. Figure 3b demonstrates that the Love mode plays an important role in the stability of shells. If $m \geq 2$, these types of instability take place.

Figure 4 shows the critical values vs thickness ratio for various lengths of shells. The transition of m at which the critical load is found is also presented. It can be seen that the critical load increases as the thickness ratio increases. There are several points on each line where the slope decreases as the thickness ratio increases. At these points, the circumferential wave number reduces to a lower value as is presented. Note that there exist some ranges along the horizontal axis where the critical load does not change with the increase of thickness ratio. These ranges are located in the region of large thickness ratios and enlarge as the length of the shell increases. In those ranges, it is seen that the flutter instability in Fig. 3a occurs and that the shell behaves like a beam. Examining Eqs. (24–27), one can see that the critical load of an equivalent beam model depends on the thickness ratio only by the shear correction factor κ. For the range of thickness ratio considered in this work, κ has an almost

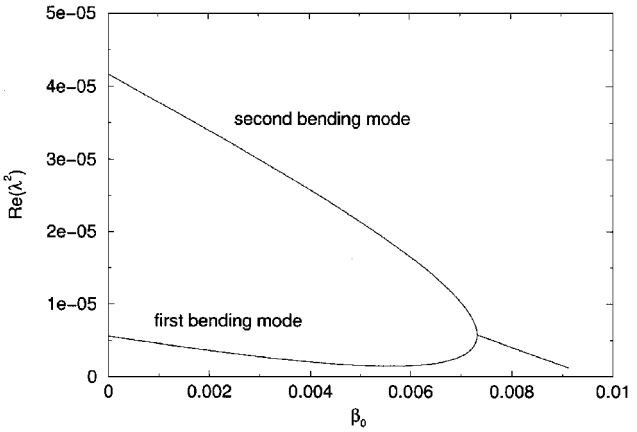

a) $h/R = 0.19$, $L/R = 80$, and $m = 1$

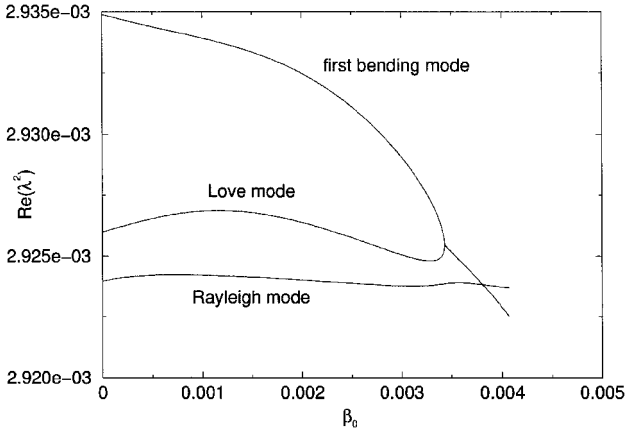

b) $h/R = 0.07$, $L/R = 70$, and $m = 2$

Fig. 3 Eigenvalue curves.

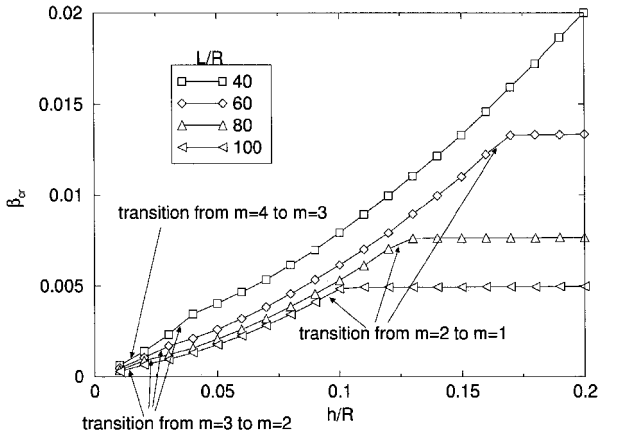

Fig. 4 Critical load vs thickness ratio.

constant value (0.53–0.57), and, therefore, the thickness ratio of the shell has little effect on the critical load of the equivalent beam. Therefore, it is probable that there exists the horizontal part in Fig. 4, but that the critical load is invariable in those ranges does not mean that the dimensional critical load remains constant. From Eq. (17), we can infer that the dimensional critical load increases linearly in those ranges, as the thickness of the shell increases with the other dimensions of the shell remaining constant.

In Fig. 5, we can compare the results of the equivalent beam model with the critical load of the beamlike flutter ($m = 1$). According to the preceding explanation regarding κ, the shear correction factor is assumed to be constant in computation of the critical load of the beam model. The critical loads for various thickness ratios merge as the length of the shell increases. The merging of the critical loads takes place because there exist some ranges where the critical load

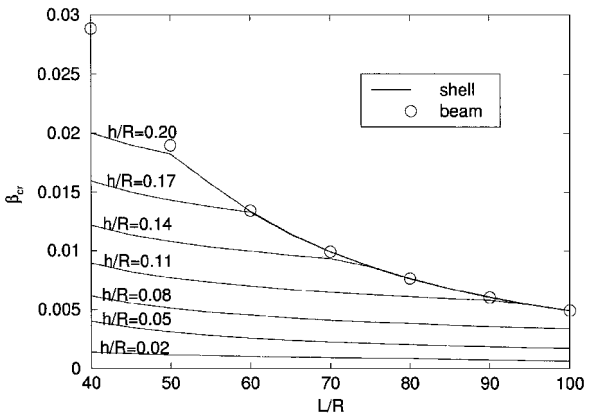

Fig. 5 Critical load vs length ratio for beam and shell.

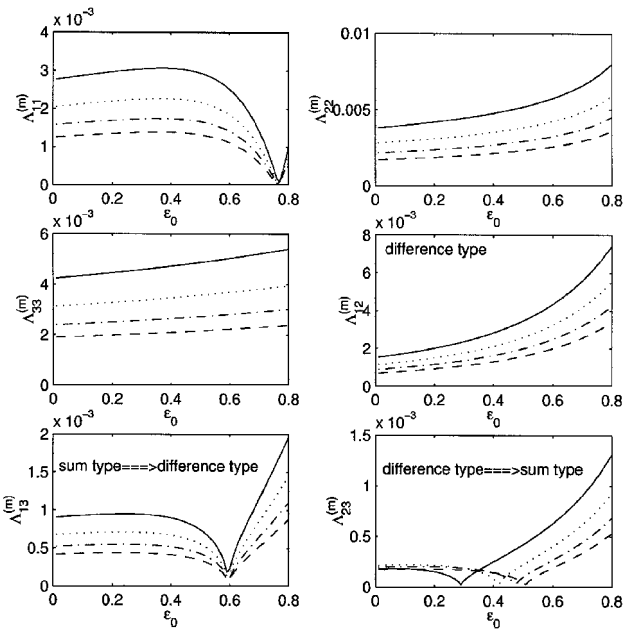

Fig. 6 Bandwidth parameter vs constant load parameter for various length ratios ($m = 1$, $h/R = 0.19$) [$L/R = 60$(——), 70(· · · ·), 80(– ·), and 90(– – –)].

does not change even though the thickness ratio increases in Fig. 4. It can be seen that the merged critical loads of shells coincide well with those of the equivalent beams. This means that a shell under a follower force might be analyzed by a beam model in the ranges of thickness and length where the beamlike modes yield the critical load.

Case $P(t) = P_0 + P_1 \cos(\omega_f t)$ (Pulsating Load)

The instability region in ϵ_1–λ_f plane for each combination of eigenvalues λ_p and λ_q can be determined by the vertex $\lambda_p \pm \lambda_q$ and the bandwidth parameter $\Lambda_{pq}^{(m)}$ for the first-order expansion as is given by Eqs. (22) and (23), where the bandwidth parameter $\Lambda_{pq}^{(m)}$ is an important factor that determines the width of unstable regions. Therefore, we focus on the bandwidth parameter in the present study. The results of the beam model are also compared with those of shells as the case of a constant follower force.

In Figs. 6 and 7 the relation between the bandwidth parameter $\Lambda_{pq}^{(m)}$ and the constant load parameter ϵ_0 is shown for various length ratios. The type of combination resonance and the transition of type is also presented. For Figs. 6 and 7, the analyzed circumferentical wave number is that inducing the critical load for the constant load case.

For the case $m = 1$, the transition of type occurs for only two combinations, $\lambda_1 \pm \lambda_3$ and $\lambda_2 \pm \lambda_3$. At the point where the transition takes place, the bandwidth parameter is 0. For the combination resonance near $\lambda_2 \pm \lambda_3$, the transition point increases as the

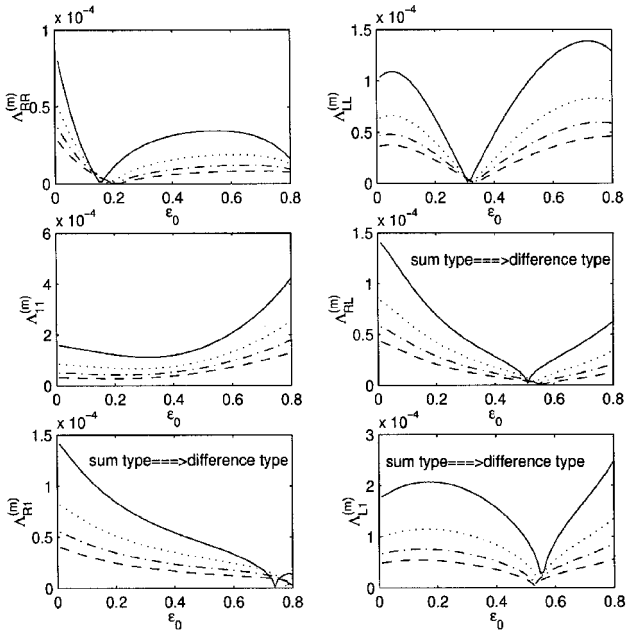

Fig. 7 Bandwidth parameter vs constant load parameter for various length ratios ($m = 2$, $h/R = 0.07$) [$L/R = 40$(——), 50(· · ·), 60(– –), and 70(– – –)].

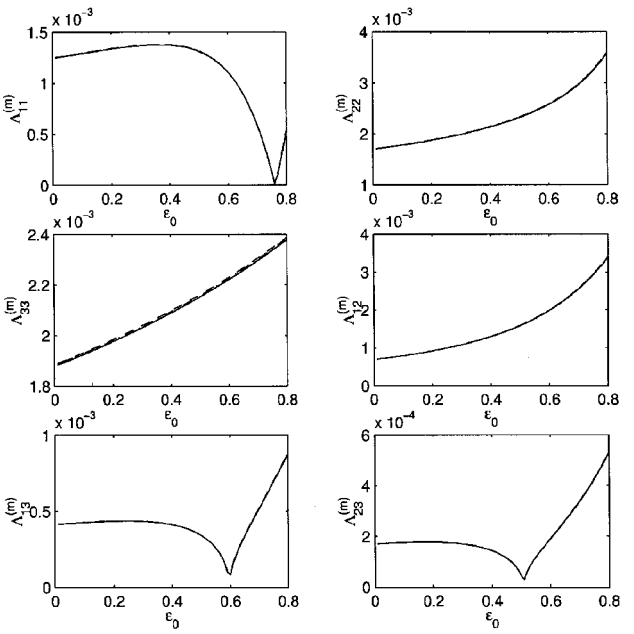

Fig. 8 Bandwidth parameter vs constant load parameter for various thickness ratios ($m = 1$, $L/R = 90$) [$h/R = 0.13$(——), 0.15(· · ·), 0.17(– –), and 0.19(– – –)].

length ratio increases. The bandwidth parameters of resonances near $2\lambda_2$, $2\lambda_3$, and $\lambda_1 - \lambda_2$ show similar tendencies. For the three resonance regions, the bandwidth parameter increases monotonically. The bandwidth parameter of resonance near $2\lambda_1$ becomes zero around $\epsilon_0 = 0.75$. Note that the eigenvalue curve of first bending mode in Fig. 3a also has a minimum eigenvalue near $\epsilon_0 = 0.75$ as is discussed in Ref. 5 for a beam model. Note also that $\Lambda_{22}^{(m)}$ and $\Lambda_{12}^{(m)}$ are relatively larger than other resonances. As for the effect of the length ratio, note that $\Lambda_{pq}^{(m)}$ decreases as the length ratio increases for the resonances near all combinations of eigenvalues as is shown in Ref. 9, where a simply supported shell under a axial force is analyzed.

The bandwidth parameters for the case $m = 2$ are shown in Fig. 7, where the subscript R and L indicate Rayleigh and Love modes, respectively. For this case, all combination resonances show the transition of type from sum type to difference type. This means that the resonance takes place in low driving frequencies, and this phenomenon is significant in the stability sense. For the resonance near $\lambda_R \pm \lambda_1$, the transition points are not apparent because they are located near $\epsilon_0 = 0.8$. The transition points of the bandwidth parameters $\Lambda_{RL}^{(m)}$ and $\Lambda_{Rl}^{(m)}$ slightly increase and those of $\Lambda_{Ll}^{(m)}$ decrease as the length ratio increases. For direct parametric resonances near $2\lambda_R$ and $2\lambda_L$, the bandwidth parameter has zero value at specific values of ϵ_0 and starts to decrease near the critical load. The specific value ϵ_0, at which $\Lambda_{RR}^{(m)}$ and $\Lambda_{LL}^{(m)}$ become zero, increases slowly as the length ratio increases. In addition, the specific value of ϵ_0 coincides approximately with the constant load β_0 at which the eigenvalue curves of the Rayleigh and Love modes have a maximum in Fig. 3b, where the maximum point of the curve of the Rayleigh mode is not apparent because the eigenvalue of the Rayleigh mode has little variation compared with those of other modes. As for the effect of the length ratio, the bandwidth parameter decreases as the length ratio increases for the resonances near all combinations of eigenvalues, which is analogous to the case $m = 1$. Note that the bandwidth of resonance near $2\lambda_{11}$ is remarkably large, and we can easily infer the reason from the mode shapes. The Rayleigh and Love modes have approximately constant and linear variations in the longitudinal direction as is explained in the previous case $P(t) = P_0$. Examining Eq. (7), we can see that a follower force has a strong effect on longitudinal bending deformations. Therefore, the first bending mode is affected more by a follower force than are the Rayleigh and Love modes.

In Figs. 8 and 9, the relation between the bandwidth parameter $\Lambda_{pq}^{(m)}$ and the constant load parameter ϵ_0 is shown for various thickness ratios. For the case $m = 1$, all four lines are so identical with one another that they cannot be distinguished. This phenomenon is corresponding to the critical load being invariable in some ranges for the case of constant follower force as shown in Fig. 4.

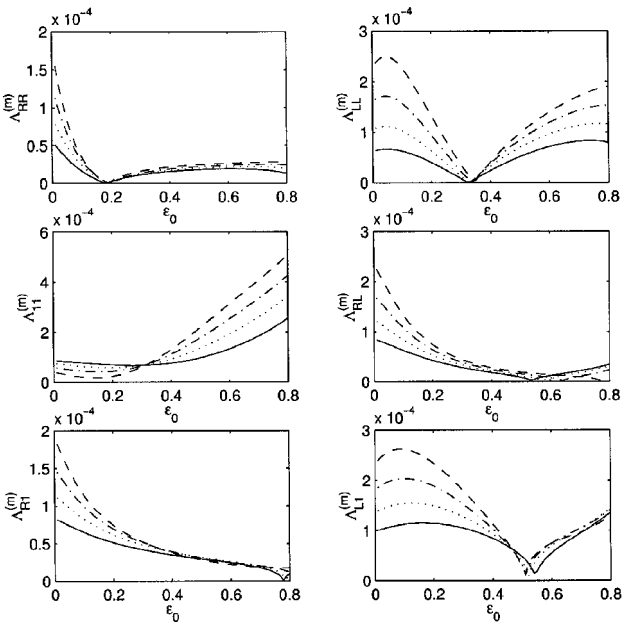

Fig. 9 Bandwidth parameter vs constant load parameter for various thickness ratios ($m = 2$, $L/R = 50$) [$h/R = 0.07$(——), 0.09(· · ·), 0.11(– –), and 0.13(– – –)].

For the case $m = 2$, the effects of thickness ratio are apparent in Fig. 9. The transition points of the bandwidth parameters $\Lambda_{RL}^{(m)}$ and $\Lambda_{Rl}^{(m)}$ increase and those of $\Lambda_{Ll}^{(m)}$ decrease as the thickness ratio increases. As for the effect of the thickness ratio, contrary to the effect of length ratio, $\Lambda_{pq}^{(m)}$ increases as the thickness ratio increases for the resonances near all combination of eigenvalues, except for some ranges in $\Lambda_{11}^{(m)}$.

Figure 10 shows the results of a beam model equivalent to the shell model used in Fig. 6. It can be seen that the bandwidth parameters are almost equal to those of the shell model. In Fig. 11, we can compare the bandwidth parameters between the two models. Note that the bandwidth parameter of a shell model is a little larger or smaller

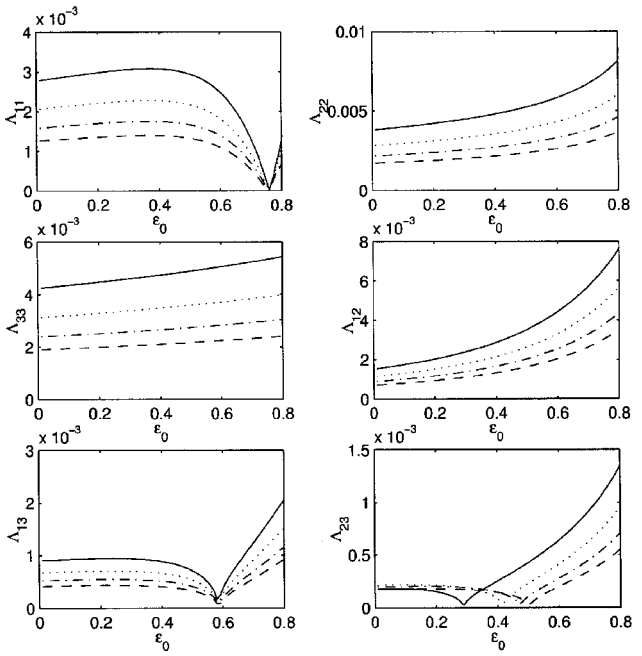

Fig. 10 Bandwidth parameter vs constant load parameter for beam model [$L/R = 60$(——), 70(· · ·), 80(– –), and 90(– – –)].

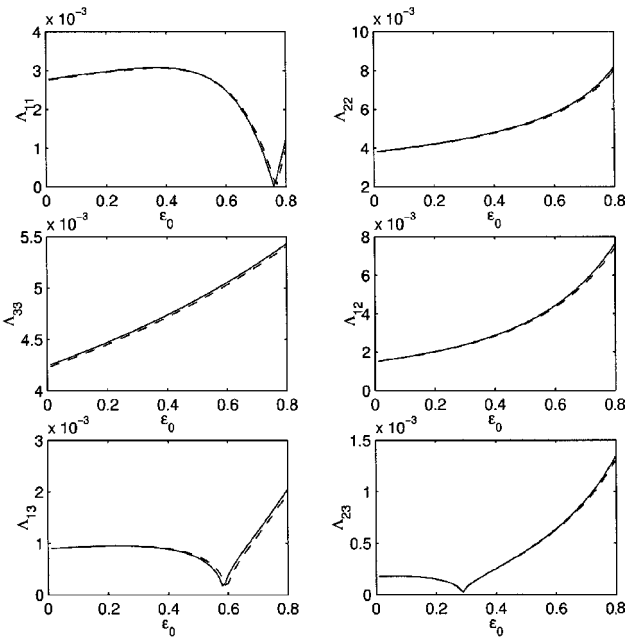

Fig. 11 Comparison of the bandwidth parameters between shell ($m = 1$, $h/R = 0.19$) and beam model ($L/R = 60$) [shell model(– – –) and beam model (——)].

than that of a beam model according to whether the bandwidth parameters increase or decrease along the horizontal axis ϵ_0.

Though comparison between the results of each model shows good agreement, the case $m = 2$ or higher also yields the instability region for shells. Therefore, the bandwidth parameter of each m should be compared with the others to determine which modes are dominant in the stability sense. Figures 12a and 12b show the ratio of the maximum bandwidth parameter of $m = 1$ and 2. Finding the maximum bandwidth parameter for each m, we consider resonances near the combinations of only the first three eigenvalues. Note that the maximum bandwidth parameter of $m = 1$ is much larger than that of $m = 2$. This means that the beamlike modes are important in the sense of parametric instability for the dimensions of shells considered in this work. Note also that the ratio increases as ϵ_0 and L/R increase in most ranges. The effect of thickness ratio is not monotonic, and the increase of h/R enhances or reduces the ratio of the maximum bandwidth parameters according to L/R and ϵ_0.

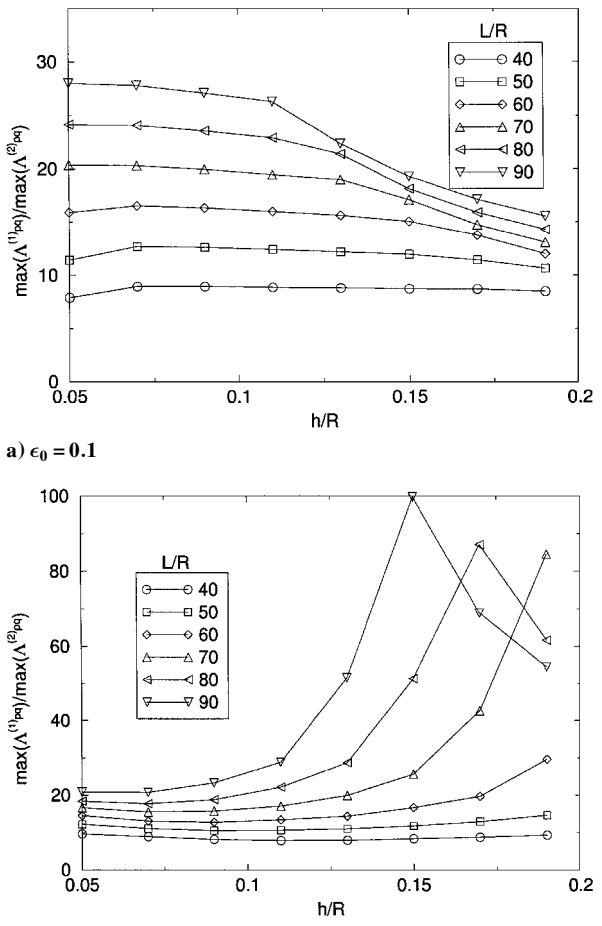

Fig. 12 Ratio of maximum Λ_{pq}.

Conclusion

A completely free cylindrical shell under a follower force has been investigated, and the results were compared with those of the corresponding beams. The cases of a constant load and a pulsating load were considered. For the case of a constant load, the critical forces of a shell model agreed well with those of a beam model in some ranges where beamlike flutter occurs. For the case of a pulsating load, the instability regions for $m = 1$ showed little difference from those of a beam model, and the instability regions of $m = 1$ were much larger than those of $m = 2$. However, the $m = 2$ modes exhibited the transition of resonance type from sum type to difference type, and this phenomenon demonstrates the importance of higher modes in the stability analysis. As a consequence of the present analysis, a shell structure can be analyzed by a beam model if the $m = 1$ modes are dominant beyond other modes in the stability sense.

Acknowledgment

This work was supported by the Korean Ministry of Education (Mechanical Engineering: ME 97-G-03).

References

[1]Beal, T. R., "Dynamic Stability of a Flexible Missile Under Constant and Pulsating Thrust," *AIAA Journal*, Vol. 3, No. 3, 1965, pp. 486–494.

[2]Wu, J. J., "On the Missile Stability," *Journal of Sound and Vibration*, Vol. 49, No. 1, 1976, pp. 141–147.

[3]Park, Y. P., and Mote, C. D., "The Maximum Controlled Follower Force on a Free–Free Beam Carrying a Concentrated Mass," *Journal of Sound and Vibration*, Vol. 98, No. 2, 1985, pp. 247–256.

[4]Park, Y. P., "Dynamic Stability of a Free Timoshenko Beam Under a Controlled Follower Force," *Journal of Sound and Vibration*, Vol. 113, No. 3, 1987, pp. 407–415.

[5]Kim, J. H., and Choo, Y. S., "Dynamic Stability of a Free–Free Timoshenko Beam Subjected to a Pulsating Follower Force," *Journal of Sound and Vibration*, Vol. 216, No. 4, 1998, pp. 623–636.

[6]Higuchi, K., and Dowell, E. H., "Dynamic Stability of a Rectangular Plate with Four Free Edges Subjected to a Follower Force," *AIAA Journal*, Vol. 28, No. 7, 1990, pp. 1300–1305.

[7]Higuchi, K., and Dowell, E. H., "Effect of Structural Damping on Flutter of Plates with a Follower Force," *AIAA Journal*, Vol. 30, No. 3, 1992, pp. 820–825.

[8]Kim, J. H., and Park, J. H., "On the Dynamic Stability of Rectangular Plates Subjected to Intermediate Follower Force," *Journal of Sound and Vibration*, Vol. 209, No. 5, 1998, pp. 882–888.

[9]Lam, K. Y., and Ng, T. Y., "Dynamic Stability of Cylindrical Shells Subjected to Conservative Periodic Axial Loads Using Different Shell Theories," *Journal of Sound and Vibration*, Vol. 207, No. 4, 1997, pp. 497–520.

[10]Bismarck, M. N., "Dynamic Stability of Shallow Shells Subjected to Follower Forces," *AIAA Journal*, Vol. 33, No. 2, 1995, pp. 355–360.

[11]Blevins, R. D., *Formulas for Natural Frequency and Mode Shape*, Litton Educational Publishing, New York, 1979, pp. 314–317.

[12]Bhimaraddi, A., "A High Order Theory for Free Vibration Analysis of Circular Cylindrical Shells," *International Journal of Solids and Structures*, Vol. 20, No. 7, 1984, pp. 623–630.

[13]Soedel, W., *Vibrations of Shells and Plates*, Marcel Dekker, New York, 1993, pp. 272–287.

[14]Meirovitch, L., *Analytical Methods in Vibrations*, Macmillan, New York, 1967, pp. 445–453.

[15]Nayfeh, A. H., and Mook, D. T., "Parametric Excitation of Linear Systems Having Many Degrees of Freedom," *Journal of the Acoustical Society of America*, Vol. 62, No. 2, 1977, pp. 375–381.

[16]Shames, I. H., and Dym, C. L., *Solid Mechanics*, McGraw–Hill, New York, 1973, pp. 187–194.

A. N. Palazotto
Associate Editor